

Effects of Multipath and Signal Blockage on GPS Navigation in the Vicinity of the International Space Station (ISS)

DAVID E. GAYLOR
Emergent Space Technologies, Inc., Greenbelt, Maryland

E. GLENN LIGHTSEY
The University of Texas at Austin, Austin, Texas

KEVIN W. KEY
Titan Corporation, Houston, Texas

Received August 2004; Revised April 2005

ABSTRACT: *Previous studies examining GPS relative navigation for spacecraft performing rendezvous with the International Space Station (ISS) have not accounted for degradation in GPS navigation performance due to multipath or blockage of GPS signals by the ISS. This study analyzes these effects on GPS navigation in the vicinity of the ISS. A simulation of a spacecraft GPS receiver operating near the ISS has been developed. This simulation includes orbit models for the GPS constellation, the ISS, and the spacecraft, as well as models for GPS signal blockage and multipath. The blockage simulation shows that aiding of GPS is required when the spacecraft approaches within 60 m of the ISS. The multipath simulation shows the expected trends in range errors as a function of GPS satellite elevation angle, distance from the ISS, number of multipath rays, and the radar cross-sectional area of the ISS.*

INTRODUCTION

Previous studies have examined GPS relative navigation for spacecraft performing rendezvous and docking with the International Space Station (ISS) [1, 2]. However, these studies have not accounted for degradation in GPS navigation performance due to multipath signals being reflected off the ISS or blockage of GPS signals by the ISS, as shown in Figure 1. Other studies have examined the multipath environment for GPS receivers on board the ISS using the uniform geometric theory of diffraction [3–5]. However, this approach is numerically intensive and not well suited to modeling a rendezvous scenario.

The objective of this study is to analyze these effects on GPS navigation in the vicinity of the ISS using simple models for GPS signal blockage and multipath. In addition to predicting GPS navigation performance in the vicinity of the ISS, these models were developed to predict the performance obtained

by combining various sensors, such as star trackers or inertial measurement units, with GPS for navigation or attitude determination.

ISS SIGNAL BLOCKAGE MODEL

It has been hypothesized that the ISS will block GPS signals needed by other spacecraft (referred to as chaser spacecraft or chasers) to navigate during rendezvous operations. To analyze this effect, the GPS signal blockage due to the ISS is modeled as a sphere centered at the ISS position with diameter $d = 100$ m.

Figure 2 depicts the various vectors used in the model. The line-of-sight vector from the chaser spacecraft to the j -th GPS satellite can be found by

$$\boldsymbol{\rho}_j = \mathbf{r}_{\text{GPS}_j} - \mathbf{r} \quad (1)$$

The line-of-sight vector from the chaser to the ISS can be found by

$$\boldsymbol{\rho}_{\text{ISS}} = \mathbf{r}_{\text{ISS}} - \mathbf{r} \quad (2)$$

The GPS antenna of the chaser spacecraft is assumed to be pointed along the \mathbf{r} vector; therefore,

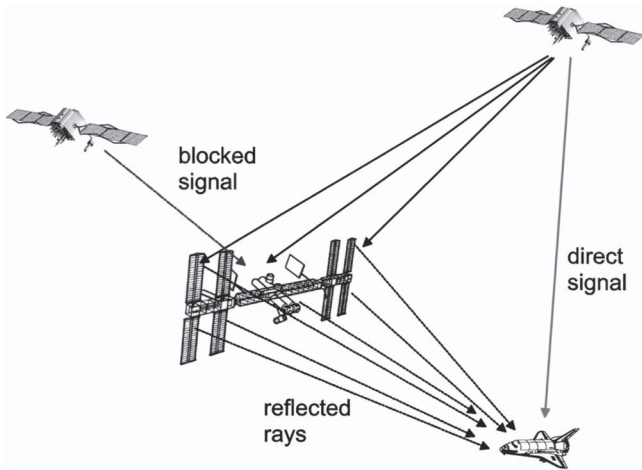


Fig. 1—ISS Blockage and Multipath Scenario

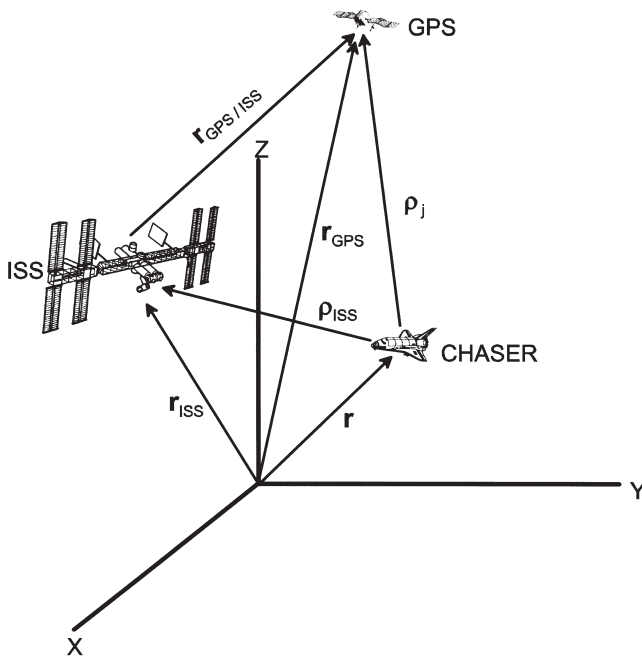


Fig. 2—Vector Definitions

the declination angle (θ) between the antenna boresight and the line-of-sight vector can be found by

$$\cos\theta_j = \frac{\mathbf{r} \cdot \boldsymbol{\rho}_j}{r \cdot \rho_j} \quad (3)$$

where $r = |\mathbf{r}|$ and $\rho_j = |\boldsymbol{\rho}_j|$.

The region of GPS signal blockage is defined by a cone about the ISS line-of-sight vector. The central angle of the cone, γ , is determined by the radius of the blockage sphere and the distance from the chaser to the ISS as follows:

$$\tan(\gamma) = \frac{d/2}{\rho_{ISS}} \quad (4)$$

where $\rho_{ISS} = |\boldsymbol{\rho}_{ISS}|$.

The angle between the GPS line-of-sight vector and the ISS line-of-sight vector can be found by:

$$\cos\chi_j = \frac{\boldsymbol{\rho}_{ISS} \cdot \boldsymbol{\rho}_j}{\rho_{ISS} \cdot \rho_j} \quad (5)$$

If the angle χ_j is less than γ , the signal will be within the blockage cone and considered to be blocked. Additionally, any GPS signals below a 10 deg minimum elevation angle from the horizontal plane, which is perpendicular to the antenna boresight vector, are also considered to be blocked. A side view of the GPS signal blockage model is shown in Figure 3. The shaded areas represent the regions where the GPS signals are blocked.

While the ISS is not actually a sphere, and GPS signals will be received from within the sphere, it is likely that those signals will be corrupted by multipath. This multipath may be severe enough to warrant programming the GPS receiver to ignore all GPS signals within the blockage cone.

ISS MULTIPATH MODEL

For spacecraft operating in the vicinity of the ISS, GPS signals may be degraded by multipath signals being reflected off the ISS. It is difficult to model the effects of these multipath signals because the ISS is composed of several reflective surfaces, some of which are moving relative to the ISS main body. Furthermore, the chaser spacecraft is moving relative to the ISS, and both are moving relative to the GPS constellation. A geometrical multipath model would have to account for each reflecting surface and the relative motion among the ISS, the chaser spacecraft, and the GPS satellites. This would be computationally intensive and not practical for use in some applications,

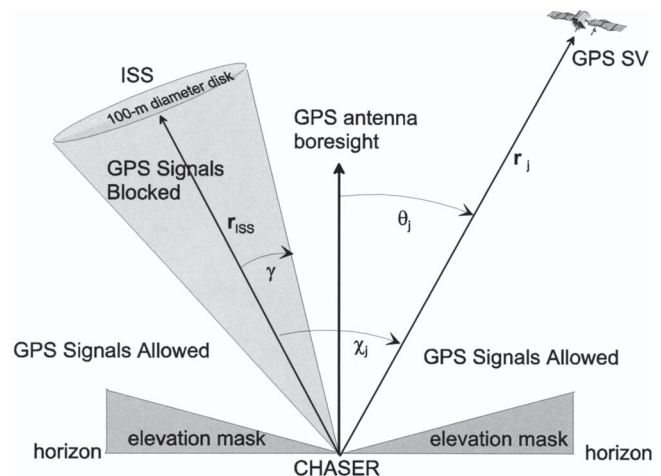


Fig. 3—GPS Signal Blockage Model

such as an integrated GPS/inertial navigation system (INS) navigation simulation of a rendezvous scenario. Therefore, a statistical multipath model was selected instead of a geometrical multipath model.

The following assumptions are made in formulating this model:

- If a GPS signal is not blocked by the ISS, it is subject to multipath.
- For each GPS signal that is not blocked by the ISS, many reflections are caused, and there is no dominant reflector.
- The phases of the reflections are uniformly distributed over the interval $[0, 2\pi)$. The rationale for this assumption is explained later in the paper.
- The relative velocity between the chaser spacecraft and the ISS is small, so that there is no significant Doppler effect between the direct and reflected signals.

According to [6], an electromagnetic signal may reach an antenna by a single direct path or indirectly through one or more reflected paths. The presence of signals arriving at the antenna from multiple reflected paths is called multipath. Because of the extra path length they travel, multipath signals arrive at the antenna with a delay relative to the direct signal. For GPS carrier-phase measurements, multipath signals combine with the direct signal to distort the received phase. Assuming there are multiple reflections, each reflected path has an associated propagation delay and attenuation factor. Both the propagation delays and attenuation factors are time varying as a result of the relative motion and geometry of the vehicles.

Consider the transmission of an unmodulated carrier at frequency f_c . The transmitted signal can be expressed as

$$x(t) = A_0 e^{j(2\pi f_c t)} \quad (6)$$

The multipath channel consists of multiple paths or rays that have real positive gains β_k , propagation delays τ_k , and phase shifts θ_k , where k is the path index and in principle ranges from 0 to ∞ . The complex, low-pass channel impulse response is given as [7]

$$h(t) = \sum_k \beta_k e^{j\theta_k} \delta(t - \tau_k) \quad (7)$$

where $\delta(\cdot)$ is the Dirac delta function. The composite received signal is the time convolution of $x(t)$ and $h(t)$ and can be represented as [7]

$$r_c(t) = \sum_k A_0 \beta_k e^{j2\pi f_c(t - \tau_k) + \theta_k} \quad (8)$$

If the direct path term is separated out and the range of k is limited to a finite number N of multipath rays, the composite received signal becomes

$$r_c(t) = A_0 \beta_0 e^{j2\pi f_c t} + \sum_{k=1}^N A_0 \beta_k e^{j2\pi f_c(t - \tau_k) + \theta_k} \quad (9)$$

If the direct signal phase is defined as $\phi_d = 2\pi f_c t$ and the multipath relative phase shift of the k -th ray is defined as $\psi_k = 2\pi f_c \tau_k + \theta_k$, then the received signal can be expressed as

$$r_c(t) = A_0 \beta_0 e^{j\phi_d} + \sum_{k=1}^N A_0 \beta_k e^{j(\phi_d + \psi_k)} \quad (10)$$

GPS Carrier-Phase Measurement Errors

The error in the carrier-phase measurement, $\delta\phi$, due to multipath, assuming the error is small, can be approximated by [8]

$$\tan \delta\phi = \frac{\sum_{k=1}^N A_0 \beta_k \sin \psi_k}{A_0 \beta_0 + \sum_{k=1}^N A_0 \beta_k \cos \psi_k} \quad (11)$$

where A_0 represents the amplitude of the signal transmitted by the GPS satellite. Factoring out A_0 leaves

$$\tan \delta\phi = \frac{\sum_{k=1}^N \beta_k \sin \psi_k}{\beta_0 + \sum_{k=1}^N \beta_k \cos \psi_k} \quad (12)$$

GPS C/A-Code Measurement Errors

The error due to multipath in GPS coarse/acquisition (C/A)-code measurements for a noncoherent GPS receiver is described in [9]. An approximation of the code correlation function is

$$R(\tau) = \begin{cases} 1 - \frac{|\tau|}{T} & |\tau| \leq T \\ 0 & |\tau| > T \end{cases} \quad (13)$$

where T is the pseudorandom noise (PRN) code bit period. The normalized form of the discriminator function with a single multipath ray is given by [9]

$$D(\tau) = R^2(\tau + \tau_d) - R^2(\tau - \tau_d) + \alpha^2 [R^2(\tau + \tau_d + \tau_m) - R^2(\tau - \tau_d + \tau_m)] + 2\alpha \cos(\psi_m) [R(\tau + \tau_d)R(\tau + \tau_d + \tau_m) - R(\tau - \tau_d)R(\tau - \tau_d + \tau_m)] \quad (14)$$

where τ is the delay lock loop (DLL) tracking error, α is the multipath relative amplitude, τ_d is the time advance of the early code or time delay of the late code (relative to the on-time code), τ_m is the multipath relative time delay, and ψ_m is the multipath relative phase angle. The τ corresponding to the zero crossing of the discriminator function is the DLL tracking error caused by multipath, which is equal

in magnitude but opposite in sign to the ranging error due to multipath.

This equation is extended in [10] to include the effects of multiple multipath rays. In this case, the discriminator function is given by

$$\begin{aligned} D(\tau) &= R^2(\tau + \tau_d) - R^2(\tau - \tau_d) \\ + 2Nk &= 1 \sum \alpha_k \cos(\psi_k) [R(\tau + \tau_d)R(\tau + \tau_d + \tau_k) \\ &\quad - R(\tau - \tau_d)R(\tau - \tau_d + \tau_k)] \\ + Nk &= 1 \sum Nl = 1 \sum \alpha_k \alpha_l \cos(\psi_k - \psi_l) \\ &\quad [R(\tau + \tau_d + \tau_k)R(\tau + \tau_d + \tau_l) \\ &\quad - R(\tau - \tau_d + \tau_k)R(\tau - \tau_d + \tau_l)] \end{aligned} \quad (15)$$

where

$$\alpha_k = \frac{\beta_k}{\beta_0} \quad (16)$$

Conjectures

Some conjectures about the nature of multipath signals have been made because limited spaceflight experiment data are available. These conjectures are based on existing terrestrial multipath models and measurements. Conjectures about the relative phase shifts, relative amplitudes, multipath power delay profile, and relative time delays are described in this section.

Phase Shifts

The multipath relative phase angle ψ_k changes by 2π when the path length changes by one wavelength. For the GPS L1 signal, $f_c = 1575.42$ MHz, the wavelength is about 19 cm. This implies that small motions of the reflector or receiver can cause ψ_k to change by 2π . The delays associated with different paths are expected to change at different rates and in an unpredictable or random manner. If one considers a fixed transmitter and a mobile receiver and imagines an ensemble of receiver positions spread over hundreds or thousands of wavelengths, then the geometry of a single path with delay τ_k will lead to a uniform distribution of phase for that path, while the geometrical relationship between separate paths with different delays will lead to a uniform joint distribution of pairs of phases, so that the phases would be independent. Therefore, the phase angles are assumed to be statistically independent random variables with a uniform distribution over $[0, 2\pi)$ [7].

Amplitudes

The received multipath signals can be modeled as random processes. When there is a large number of

paths (in practice, greater than 6), the central limit theorem may be applied so that the received signal, $r_c(t)$, can be modeled as a complex-valued Gaussian random process [7]

The received signal can be broken down into in-phase and quadrature components, $I(t)$ and $Q(t)$, which are independent Gaussian processes. This means they are completely characterized by their mean value and autocorrelation function. $I(t)$ and $Q(t)$ have equal variance σ^2 equal to the mean square power. The total amplitude of the signal is the square root of the sum of the squares of $I(t)$ and $Q(t)$, which are Gaussian. This leads to the conjecture that the amplitudes are Rayleigh distributed. Therefore, the β_k 's are Rayleigh distributed such that

$$p(\beta_k^2) = \frac{1}{\bar{\beta}_k^2} e^{-\left(\beta_k^2/\bar{\beta}_k^2\right)} \quad (17)$$

where $\bar{\beta}_k^2 =$ the average power gain at τ_k [11].

Power-Delay Profile

The multipath power-delay profile for a given environment is the expected power received as a function of delay. Numerous measurements of the multipath power-delay profile for various environments have been made, such as those in [12] and [13]. Based on these studies, a general model of the multipath average power-delay profile can be given as [14]

$$\bar{P}(\tau) = P_0 e^{-\tau\bar{\tau}} \quad (18)$$

where $\bar{\tau}$ is the mean excess delay of the multipath reflections, and P_0 is the total multipath power. The total multipath power is estimated by using the bistatic radar equation

$$P_0 = \frac{A_{RCS} \lambda^2 G_r^{mp} P_t G_t}{(4\pi)^3 \rho_{ISS} r_{GPS/ISS}^2} \quad (19)$$

where ρ_{ISS} is the distance from the spacecraft to the ISS, $r_{GPS/ISS}$ is the distance from the ISS to the GPS satellite, A_{RCS} is the radar cross-sectional area of the ISS, λ is the wavelength, G_r^{mp} is the antenna gain of the receiver in the direction of the multipath, and $P_t G_t$ is the effective isotropic radiated power from the GPS satellite.

The average power in each multipath signal is

$$\bar{P}_k = \frac{1}{2} A_0^2 \bar{\beta}_k^2 \quad (20)$$

Equating this with equation (18) and solving for $\bar{\beta}_k^2$ leads to

$$\bar{\beta}_k^2 = \frac{2P_0}{A_0^2} e^{-\tau\bar{\tau}} \quad (21)$$

Substituting equation (19) into equation (21) and recognizing that $A_0^2 = 2P_t G_t$ results in the following expression:

$$\bar{\beta}_k^2(\tau) = \frac{A_{RCS} \lambda^2 G_r^{mp}}{(4\pi)^3 \rho_{ISS}^2 r_{GPS/ISS}^2} e^{-\tau} \quad (22)$$

Since the multipath rays are being reflected off the ISS, the mean excess delay is approximated by

$$\bar{\tau} = \frac{\rho_{ISS}}{c} \quad (23)$$

where c is the speed of light. The power of the direct signal is estimated by using the Friis equation:

$$P_{direct} = \frac{1}{2} A_0^2 \beta_0^2 = \frac{\lambda^2 G_r^{direct} P_t G_t}{(4\pi \rho_j)^2} \quad (24)$$

Since $A_0^2 = 2P_t G_t$,

$$\beta_0^2 = \frac{\lambda^2 G_r^{direct}}{(4\pi r_{GPS/STS})^2} \quad (25)$$

If a cardioid pattern antenna is used, then

$$G_r^{direct} = 1 + \cos \theta_{direct} \quad (26)$$

where θ_{direct} is the angle between the direct line-of-sight vector and the antenna boresight vector. Substituting equation (26) into equation (25) leads to

$$\beta_0 = \sqrt{\frac{\lambda^2 (1 + \cos \theta_{direct})}{(4\pi \rho_j)^2}} \quad (27)$$

Delay Times

The mean excess delay and root mean square (RMS) delay spread are commonly used to characterize multipath time delays. The parameters are determined from a multipath power delay profile. The mean excess delay is the first moment of the power delay profile and is defined as [15]

$$\bar{\tau} = \frac{\sum_k \beta_k^2 \tau_k}{\sum_k \beta_k^2} \quad (28)$$

In [16], it is proposed that the delay times form a Poisson sequence. The probability distribution of time delays is given by [17]

$$p(\tau_k) = \frac{1}{\bar{\tau}} e^{-\frac{\tau_k}{\bar{\tau}}} \quad (29)$$

Multipath Model Algorithm

The algorithm for calculating the multipath error for each GPS measurement is as follows:

1. For each simulation time and each GPS satellite, compute \mathbf{r} , $\mathbf{r}_{GPS/ISS}$, and θ_{direct} .
2. Compute β_0 using equation (27) and $\bar{\tau}$ using equation (23).

3. Given N , obtain the τ_k 's from the Poisson distribution given in equation (29).
4. For each τ_k :
 - a. Given A_{RCS} , compute $\bar{\beta}_k^2$ using equation (22).
 - b. Obtain the β_k 's from the Rayleigh distribution given in equation (17).
 - c. Obtain the ψ_k 's from a uniform distribution over $[0, 2\pi)$.
 - d. Construct $\beta_k \sin \psi_k$ and $\beta_k \cos \psi_k$.
5. Determine the carrier-phase range error from equation (12).
6. Determine the code range error from equation (15).

SIMULATION ORBIT MODELS

The orbit models used for the simulation of the GPS constellation, ISS, and chaser spacecraft are presented in this section.

GPS Constellation Model

A model of the GPS constellation was constructed from a daily global broadcast ephemeris file in the Receiver Independent Exchange (RINEX) format downloaded from the National Geodetic Survey (NGS) Continuously Operating Reference Stations (CORS) website. This file contains the GPS broadcast ephemeris parameters for each satellite in the constellation for March 1, 2001. There were a total of 28 satellites in the active constellation. The ephemeris parameters and the equations used to determine the positions of the GPS satellites at a given time are described in the [18]. This GPS constellation model was used for all simulations in this study.

ISS and Chaser Spacecraft Orbit Models

The ISS orbit model was an unperturbed two-body orbit with orbit elements presented in Table 1. To determine the GPS signal blockage, the chaser spacecraft was positioned so that it remained at a constant distance Δr directly below the ISS along the radius vector from the center of the earth to the ISS. Δr was varied for each simulation run to determine the GPS signal blockage and multipath effects at different distances below the ISS. While this does not represent a rendezvous scenario, it allows a large number of samples to be collected over the course of the simulation while maintaining the same geometry relative to the ISS. Another reason for placing the chaser at various distances below the ISS is to evaluate the blockage at different points during an R-bar approach in which the chaser approaches the ISS along the earth to the ISS radius vector.

Table 1—ISS Orbit Elements

Element	Value
a	6678.0 km
e	0.005
i	56.0 deg

ISS BLOCKAGE STUDY RESULTS

The results of the computer simulation developed to study the GPS signal blockage due to the ISS are presented in this section.

Two kinds of GPS receivers were modeled. The first was an all-in-view receiver that is able to track all visible GPS satellites with no delay in acquisition and tracking of a satellite as soon as it becomes visible. The second was a 12-channel receiver programmed to track the twelve highest-elevation space vehicles (SVs). For this receiver, it was also assumed to have no delay in tracking a satellite as soon as it becomes visible.

The simulation was run over a time span of 1 day, with samples taken once/s for the following values of Δr : 10, 20, 30, 40, 50, 60, and 100 m. At each point in time, the number of visible GPS satellites was recorded and analyzed. Whenever fewer than four GPS satellites were visible, this was considered to be an outage. The data collected on outages for the all-in-view receiver are summarized in Table 2.

The data show that at least four GPS satellites were in view at all times when the chaser was 100 m or more below the ISS. At 60 m below the ISS, there were fewer than four satellites in view for a small percentage of the time, but the average outage was over 102 s long. The amount of blockage increased as the chaser was brought closer to the ISS. When it was 10 m below the ISS, no GPS position fixing was possible. These results suggest that aiding of GPS is needed when a chaser spacecraft is within 60 m of the ISS.

The 12-channel receiver results were almost identical to the all-in-view receiver results. The only difference was that the number of satellites below the horizon mask was higher for the all-in-view receiver. Therefore, the number of visible GPS SVs for a 12-channel receiver programmed to select the 12 highest-elevation SVs was the same as for an all-in-view receiver.

Table 2—GPS Signal Outage Statistics (all-in-view receiver)

Meters Below ISS	% Outage Duration (s)	Max. Outage Duration (s)	Avg. Outage Duration (s)
10	99.99	58059.0	43197.0
20	85.85	2111.0	501.2
30	42.04	1119.0	167.4
40	12.79	602.0	107.3
50	4.92	389.0	103.6
60	2.38	249.0	102.8
100	0.0	0.0	0.0

MULTIPATH STUDY RESULTS

The multipath model described in this paper was added to the ISS signal blockage simulation. The carrier-phase and code-range errors for each channel of an all-in-view GPS receiver were computed and converted to meters. Time histories for the carrier-phase and code-range errors for channel 1 of this receiver were computed for various values of Δr to determine the behavior as the chaser approaches the ISS. The values of N and A_{RCS} were also varied to determine the sensitivity to these two model tuning parameters. τ_d was one-half of the C/A-code chip period. The errors were computed and recorded once/s for 3600 s.

Geometry Dependence

The errors due to multipath are dependent on the GPS satellite geometry because a stronger direct signal is less susceptible to multipath. Higher-elevation signals are stronger because the receiving antenna gain is higher, and the GPS satellite is closer to the receiver. Both of these effects are accounted for in equation (27).

The time history of carrier-phase and C/A-code range errors and the corresponding direct signal elevation angles are shown in Figure 4. As expected, the magnitude of the range errors increases as the direct signal elevation decreases.

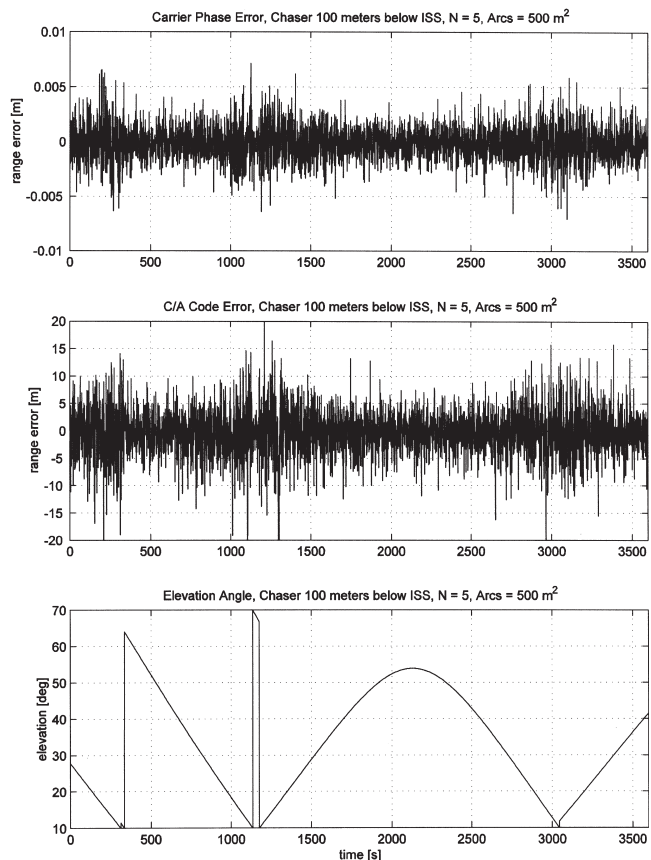


Fig. 4—Range Errors and Direct Signal Elevation Angles

Distance from ISS

It is expected that the range errors due to multipath will increase as the spacecraft approaches the ISS. This effect is evident in the time histories of carrier-phase and C/A-code range errors at 50, 100, and 200 m below the ISS, as shown in Figures 5 and 6, respectively.

Number of Multipath Rays

One of the model parameters is the number of multipath rays per GPS signal. The number of reflected rays would be expected to increase as more modules, solar arrays, and thermal radiators are added to the ISS. It is expected that the range errors due to multipath will increase as the number of multipath rays (N) increases. This trend is seen in the time histories of carrier-phase and C/A-code range errors at 100 m below the ISS shown in Figures 7 and 8, respectively.

ISS Radar Cross-sectional Area

The ISS radar cross-sectional area is another model parameter. It acts as a scaling factor on the total received multipath power and can be used to account for the reflective properties and size of the various ISS

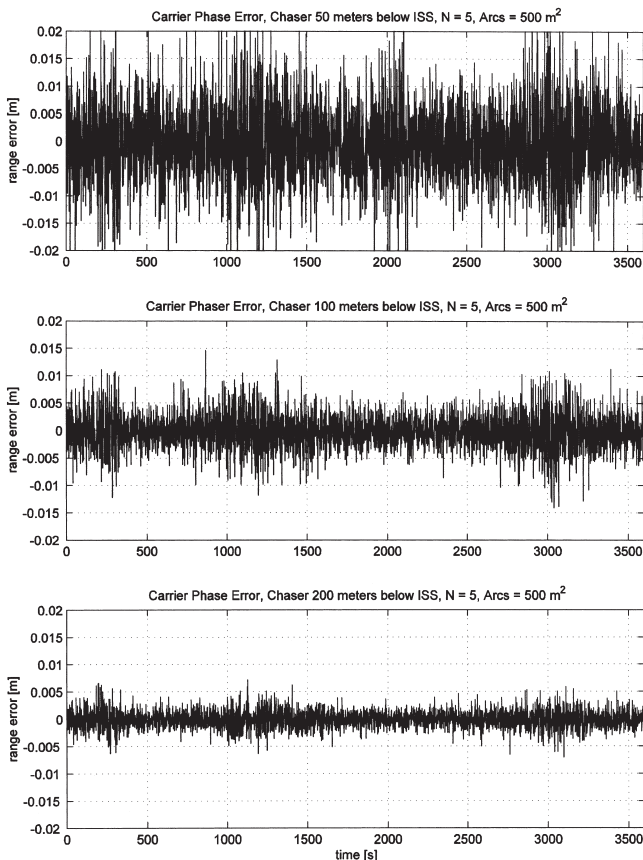


Fig. 5—Carrier-Phase Range Errors at 50, 100, and 200 m below the ISS

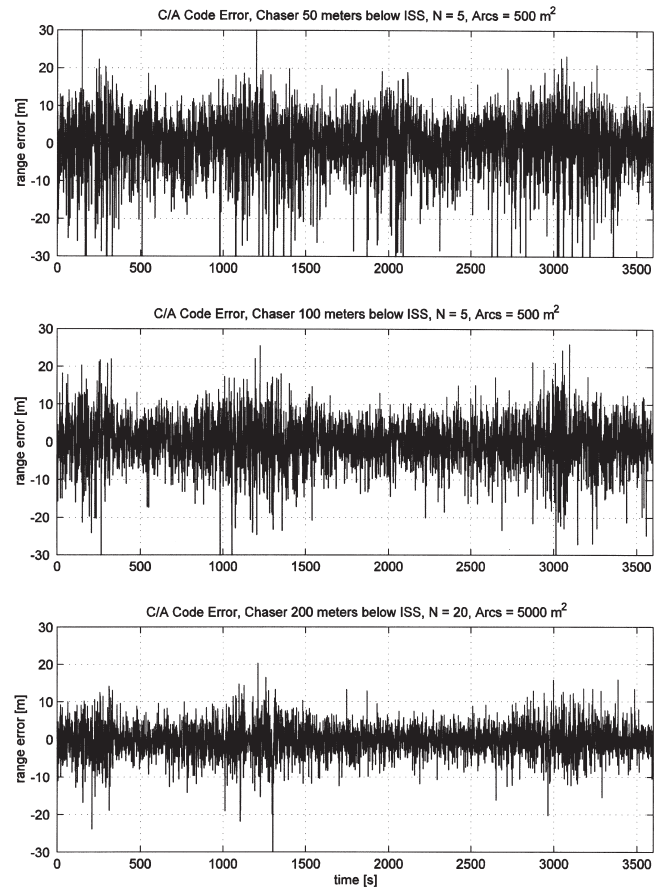


Fig. 6—C/A-Code Range Errors at 50, 100, and 200 m below the ISS

structures. The radar cross-sectional area would be expected to increase as more modules, solar arrays, and thermal radiators are added to the ISS. The range errors due to multipath are expected to increase as the ISS radar cross-sectional area (A_{RCS}) increases. This effect is seen in the time histories of carrier-phase and C/A-code range errors at 100 m below the ISS in Figures 9 and 10, respectively.

Model Tuning

The following parameters can be used to tune the multipath model: the ISS radar cross-sectional area, the number of multipath reflections per direct signal, and the direct signal antenna gain. As more modules, solar arrays, and thermal radiators are added to the ISS, its radar cross-sectional area and the number of multipath reflections are expected to increase. Therefore, the multipath model can readily adjust to the changing configuration of the ISS over time.

CONCLUSIONS

Models of the GPS blockage and multipath effects near the ISS have been developed. These models have been incorporated into a simulation to show

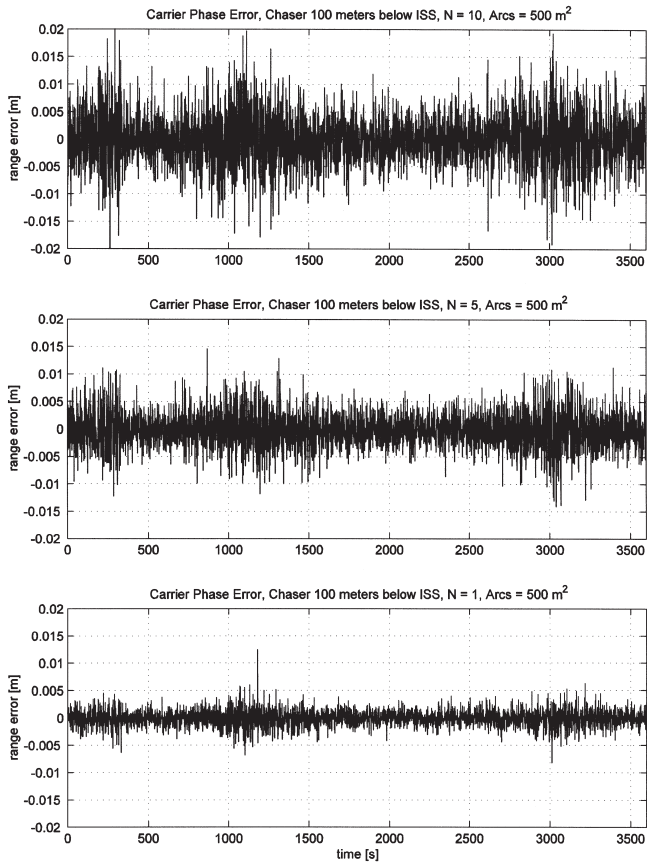


Fig. 7—Carrier-Phase Range Errors with Various Numbers of Multipath Rays

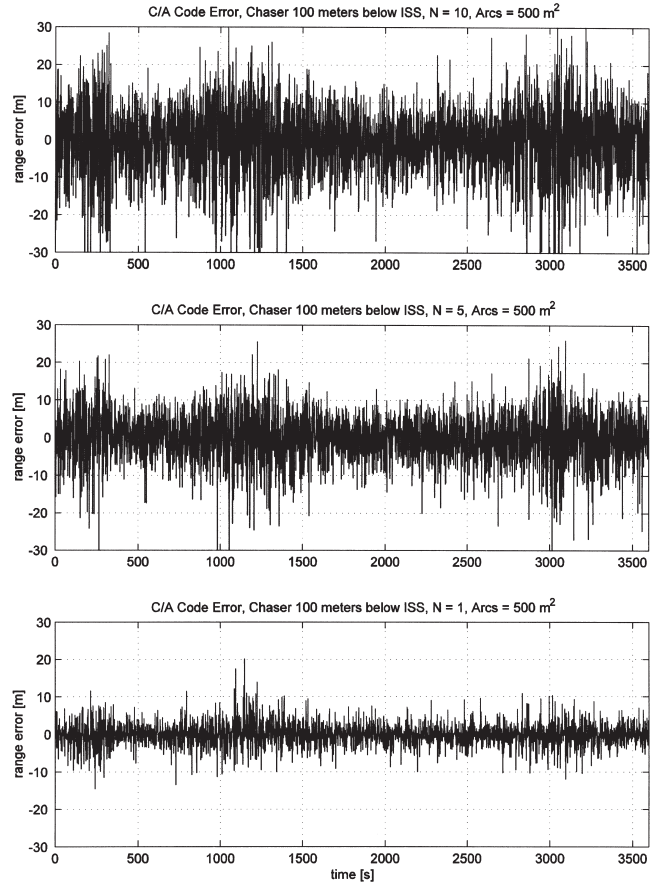


Fig. 8—C/A-Code Range Errors with Various Numbers of Multipath Rays

how GPS signal blockage and multipath impact GPS navigation in the vicinity of the ISS. The blockage simulation shows that aiding of GPS is needed when the spacecraft approaches within 60 m of the ISS. The multipath simulation results show the expected trends in the range errors as a function of the GPS satellite elevation angle, the distance from the ISS, the number of multipath rays modeled, and the radar cross-sectional area of the ISS. Both effects may significantly degrade GPS navigation near the ISS. These models can be used to predict the performance obtained by combining various sensors with GPS for navigation or attitude determination for spacecraft operating near the ISS or some other large reflecting body.

After consulting with engineers at the National Aeronautics and Space Administration's (NASA) Johnson Space Center, it was determined that the data needed to validate the ISS blockage and multipath models do not currently exist. Therefore, the values of the tuning parameters used in the multipath study were chosen based on anecdotal experience, not empirical data.

Since engineers are currently designing autonomous rendezvous and docking systems for the ISS using GPS, it is recommended that a flight experiment to determine the levels of GPS signal

blockage and multipath for pseudorange and carrier-phase measurements near the ISS be flown as soon as possible.

FUTURE WORK

The next logical step is to validate these models with actual flight data. If appropriate flight data cannot be found, the results of this paper could be used to justify a future flight experiment. It may also be possible to compare these results with data from other existing simulations. The conjectures that lead to the multipath model presented here have been used in developing statistical multipath models for wireless communication systems in the past [15]. However, the multipath environment near the ISS has not yet been characterized by experimental data.

If the multipath average power-delay profile, excess time delays, and delay spread were measured during a flight experiment as described in [12], the approximations from the Friis and bistatic radar equations could be replaced by curve fits. The average time-delay approximation could also be replaced by a measured value.

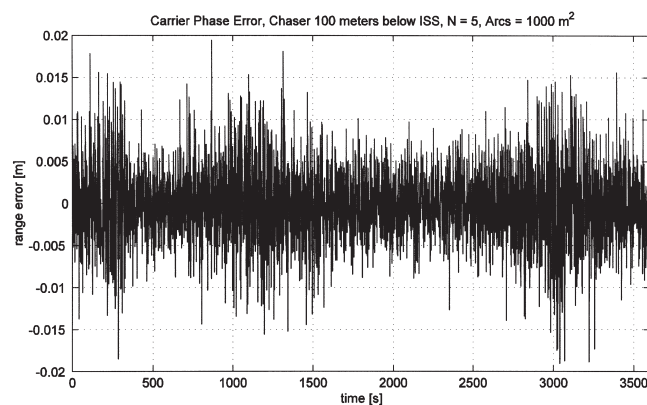
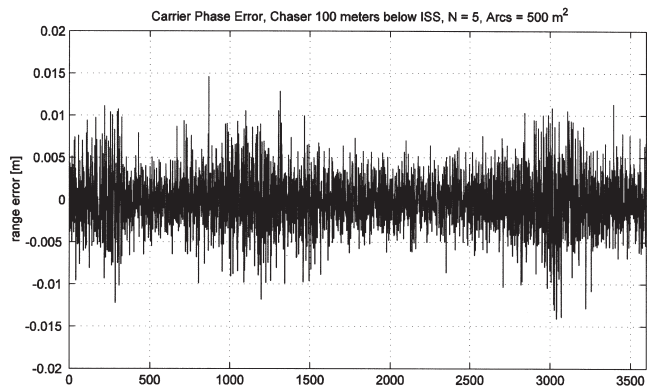


Fig. 9—Carrier-Phase Range Errors with Different ISS Radar Cross-sectional Areas

Alternatively, if GPS measurements and a very accurate reference trajectory (with errors smaller than the predicted multipath errors) were available from a flight experiment, it should be possible to adjust the number of multipath rays and ISS radar cross-sectional area to match the measured multipath-induced range errors.

A very simple GPS receiver model was used in this study. Most if not all commercially available GPS receivers smooth the pseudorange measurements using carrier-phase aiding, carrier smoothing, or both. This study yielded pseudorange and carrier-phase errors due to multipath with no smoothing applied. The analysis of multipath mitigation by the use of smoothing and other techniques is another suggested topic for future research.

ACKNOWLEDGMENTS

This research was partially funded by the NSTL Relative Navigation Support Grant (NAG9-1189) from the Navigation Systems and Technology Laboratory at NASA Johnson Space Center.

The results presented in this paper were produced using software from the Java Astrodynamics Toolkit, an open source software library available on the Internet at <http://jat.sourceforge.net>.

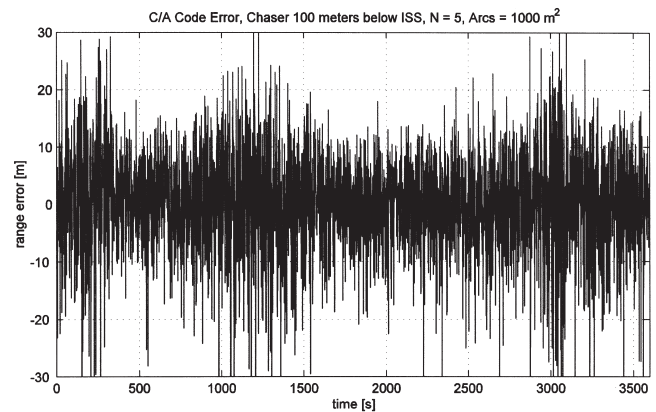
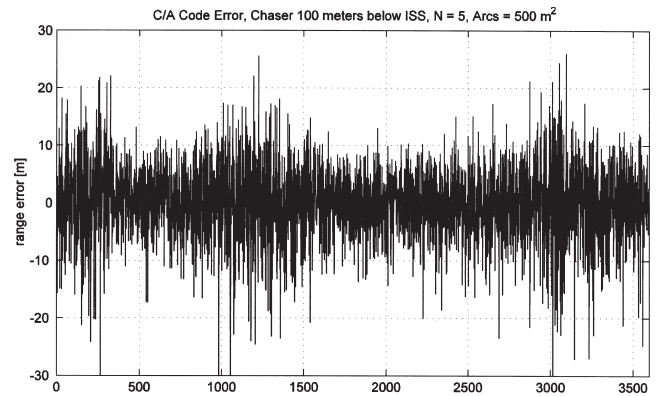


Fig. 10—C/A-Code Range Errors with Different ISS Radar Cross-sectional Areas

REFERENCES

1. Ebinuma, T., R. Bishop, and E. G. Lightsey, *Spacecraft Rendezvous Using GPS Relative Navigation*, Paper No. AAS 01-152, AAS/AIAA Spaceflight Mechanics Meeting, Santa Barbara, CA, February 2001.
2. Um, J., *Relative Navigation and Attitude Determination Using a GPS/INS Integrated System Near the International Space Station*, Ph.D. thesis, The University of Texas at Austin, December 2001.
3. Gomez, S. and S. Hwu, *Comparison of Space Shuttle GPS Flight Data to Geometric Theory of Diffraction Predictions*, Proceedings of The Institute of Navigation's ION GPS-97, September 1997.
4. Hwu, S., B. Lu, J. Hernandez, R. Panneton, S. Gomez, and P. Saunders, *A New Modeling Approach for Space Station GPS Multipath Analysis Including Dynamic Solar Panel Movements*, Proceedings of The Institute of Navigation's National Technical Meeting, 1997.
5. Byun, S., G. Hajj, and L. Young, *Assessment of GPS Signal Multipath Interference*, Proceedings of The Institute of Navigation's National Technical Meeting, 2002.
6. Comp, C., *GPS Carrier Phase Multipath Characterization and a Mitigation Technique Using the Signal-to-Noise Ratio*, Ph.D. thesis, University of Colorado, July 1996.

7. Proakis, J., *Digital Communications*, J. Wiley & Sons, New York, NY, 1989.
8. Axelrad, P., C. Comp, and P. MacDoran, *SNR-Based Multipath Error Correction for GPS Differential Phase*, IEEE Transactions on Aerospace and Electronic Systems, Vol. 32, No. 2, April 1996.
9. Braasch, M., *Multipath Effects*, Global Positioning System: Theory and Applications, Vol. 1, Chapter 14, AIAA, 1996, pp. 547–68.
10. Mora-Castro, E., C. Carrascosa-Sanz, and G. Ortega, *Characterisation of the Multipath Effects on the GPS Pseudorange and Carrier Phase Measurements*, Proceedings of The Institute of Navigation's ION GPS-98, September 1998.
11. Saleh, A. and R. Valenzuela, *A Statistical Model for Indoor Multipath Propagation*, IEEE Journal on Selected Areas in Communications, SAC-5, No. 2, February 1987.
12. Van Rees, J., *Measurements of the Wide-Band Radio Channel Characteristics for Rural, Residential and Suburban Areas*, IEEE Transactions on Vehicular Technology, VT-36, February 1987.
13. Belloul, B., S. Saunders, M. Parks, and B. Evans, *Measurement and Modelling of Wideband Propagation at L- and S-bands Applicable to the LMS Channel*, IEEE Proceedings: Microwave Antenna Propagation, Vol. 147, No. 2, April 2000.
14. Van Nee, R., *Multipath Effects on GPS Code Phase Measurements*, NAVIGATION, Journal of The Institute of Navigation, Vol. 39, No. 2, 1992.
15. Rappaport, T., *Wireless Communications: Principles and Practice*, 2nd Edition, Prentice-Hall, Inc., Upper Saddle River, NJ, 2002.
16. Turin, G., F. Clapp, T. Johnston, S. Fine, and D. Lavry, *A Statistical Model of Urban Multipath Propagation*, IEEE Transactions on Vehicular Technology, VT-21, No. 1, February 1972.
17. Lee, W., *Mobile Communications Design Fundamentals*, Howard W. Sams & Co., Indianapolis, IN, 1986.
18. GPS Program Office, *NAVSTAR GPS Space Segment/Navigation User Interfaces*, Technical Report ICD-GPS-200, ARINC Research Corporation, Fountain Valley, CA, 1997.